Doppler effect mitigation in LEO-based 5G Non-Terrestrial Networks

Ashish Kumar Meshram, Sumit Kumar, Jorge Querol, Symeon Chatzinotas
Interdisciplinary Centre for Security, Reliability and Trust (SnT), University of Luxembourg, Luxembourg
Email:{ashish.meshram, sumit.kumar, jorge.querol,symeon.chatzinotas}@uni.lu,

***Abstract*—In recent years, integrating Non-Terrestrial Networks (NTN) components with 5G Terrestrial Networks (TN) has led to considerable attention from academia and industry, leading to the standardization of 5G-NTN in 3GPP. Among the various NTN solutions, a notable one is the Low Earth Orbit (LEO)-based 5G-NTN with a regenerative payload. This system stands out because it can provide latency and throughput levels similar to terrestrial 5G networks. However, a significant challenge in this integration arises from the substantial Doppler effect caused by the rapid movement of LEO satellites. This effect must be effectively addressed to establish a successful data link between the User Equipment (UE) and the gNodeB (gNB). This study proposes a simple yet efficient method to tackle this issue. The method involves using a regenerative LEO satellite-based 5G gNB, which pre-compensates the Doppler frequency with respect to its beam center before initiating any data transmission. Subsequently, the UE performs post-compensation to handle residual Doppler frequency and achieve accurate initial synchronization. We evaluated the performance through simulations and demonstrated the effectiveness of the proposed system. The results indicate successful mitigation of Doppler effects, facilitating seamless communication between LEO satellite-based 5G NTN.**

***Index Terms*—5G New Radio, Non-Terrestrial Networks, Estimation, Doppler Shift, Compensation, Initial Synchronization**

I. Introduction

Introducing satellite components in the recent 3GPP Release-17 has accelerated the long-awaited convergence of 5G and beyond 5G TN and NTN [1], [2]. The 5G-NR protocol stack, initially designed for TN, has been selected as the technology for 5G-NTN due to its distinctive physical layer characteristics. However, integrating 5G-TN with NTN components presents complex challenges, particularly considering the effects of the high mobility of LEO satellites which cause significantly high Doppler [3]. This results in a mismatch of the Carrier Frequency Offset (CFO) between the transmitter and receiver, further increasing Inter-Carrier Interference (ICI) [4] leading to difficulties in achieving initial synchronization. Furthermore, it imposes higher complexity on receiver-side algorithms to estimate and compensate CFO and ICI. While having prior information about the satellite orbits would mitigate this challenge with a trade-off in overhead and frequent updation, obtaining such information about the regenerative satellite orbits at the UE before initial synchronization is challenging due to the dynamicity of LEO satellites, limited visibility duration, time synchronization, and ephemeris data volume constraints [5].

The majority of the past works that have addressed the Doppler effects for 5G-NTN can be categorized under Doppler characterization, propagation impairment in the LEO satellite channel, and Multple-Input Multiple-Output (MIMO). We emphasize some noteworthy solutions available and their limitations. In [6]–[12], Doppler frequency characterization relies on the two-body equation of motion without considering the effect of the satellite orbital perturbation, which can cause satellites to drift from their intended positions, affecting their ability to maintain accurate and stable communications. In [13], the Doppler shift is expressed in terms of the Taylor series up to the second term consisting of the Doppler shift and rate. The high non-linearity of the Doppler shift function poses a challenge when using a limited number of terms in the Taylor series approximation can lead to significant errors for large frequency deviations or rapid changes. Whereas [14]–[16], do not consider any prior information on Doppler characterization resulting in complex estimation and compensation algorithm at the UE. Specifically, [16] proposes an additional 5G NR Synchronization Signal Block (SSB) placement in different frequency locations, resulting in further overhead. In terms of propagation channel, most studies focus on multipath channels [7], [11], [12], [14] but fail to address the impact of large-scale fading caused by the large distance between the satellite and ground UE. This effect varies depending on the location of the UE, whether it is in densely populated or rural areas. When considering MIMO, it is essential to mention that no analytical work has been done so far, apart from the study by [16], which focused on a simulation involving a UE with two receive antennas.

We also mention two recent experimental projects, 5G-GOA [17], and 5G-LEO [18] where open-source based Software Defined Radio (SDR) framework OpenAirInterface5G has been used for over-the-satellite real-world experiments. 5G-GOA addresses challenges caused by significant delay (approx 520ms) and does not focus on Doppler. While 5G-LEO addresses the Doppler, it considers only transparent payload satellites. Moreover, 5G-LEO does not provide an analytical approach to compensate for the Doppler.

Considering the limitations mentioned above, our contributions to this work as listed below:

1. An efficient method for Doppler frequency pre-compensation at the satellite to reduce the complexity of the UE CFO estimation algorithm, where the UE does not need apriori knowledge of the satellite's ephemeris during the initial synchronization phase.
2. For an accurate estimation of residual Doppler frequency, we provide an approximate mathematical expression indicating the furthest distance a UE can deviate from the BC.
3. Finally, we provide an efficient algorithm for estimating frequency offset in the time domain, which uses Cyclic Prefix (CP) based correlation and works satisfactorily

even on low Signal-to-Noise Ratio (SNR).

Throughout this paper, we follow these notations unless specified specifically, $c = 3 \times 10^8$ (m/s) for the speed of light. Small and capital boldface symbol $\mathbf{x}, \mathbf{X}$ for complex-valued IQ samples in time- and frequency-domain, respectively. $\circledast$ for convolution and $*$ for conjugation operations, respectively. $\mathrm{U}(a, b)$ represents uniformly distributed random numbers within the range a to b. Probability is denoted as $\Pr(\cdot)$, $\mathbb{E}[\cdot]$ for Expectation operator, $f_{\mathrm{X}}(x), F_{\mathrm{X}}(x)$ for probability and cumulative distribution function of a random variable X, respectively. Furthermore, mathematical steps in obtaining final expressions have been omitted for brevity.

II. System Model

Our system model considers a scenario with a regenerative payload LEO satellite equipped with steerable spot beams fixed to the specific location on the Earth's surface, as shown in Fig. 1. Let us assume each onboard transmitter is equipped with N_{TX} number of transmit antenna, with a dedicated transmitting power P_{TX}. Furthermore, each spot beam on the satellite possesses detailed information about its designated location on the Earth's surface where the beam has to point, known as the beam center (BC). Let $\tilde{\mathbf{r}}_{\mathrm{BC}} \in \mathbb{R}^3$ in Earth-Centered, Earth-Fixed (ECEF) coordinates system denotes the BC position vector. This knowledge enables the satellite to precisely direct its spot beams towards specific points on Earth as it moves along its orbit. These spot beams are guided by onboard sensors, allowing the satellite to precisely determine its orbital position in space and maintain accurate time synchronization in ideal situations. But we assume that onboard sensors may introduce an error in pointing for an angle deviation of 0.05° [19] resulting in 5 km, which we have modeled as uniformly distributed within ± 5 km. i.e., $\mathbf{r}_{\mathrm{BC}} = \tilde{\mathbf{r}}_{\mathrm{BC}} + [\mathrm{U}(-5,5), \mathrm{U}(-5,5), \mathrm{U}(-5,5)]$. We also assume that the UE equipped with N_{RX} number of receive antenna does not have apriori information about the satellite ephemeris. Besides, neither the satellite nor the UE initially knows the location of each other before synchronization.

A. Channel Model

To capture the effects of the channel between the LEO satellite and UE, we consider a time-varying frequency-selective channel model. Let $\mathbf{h}_p^{(i,j)}(t,\tau) \in \mathbb{C}^{N_{\mathrm{RX}} \times N_{\mathrm{TX}}}$ denotes the channel impulse response for the p-th UE as

$$\mathbf{h}_p^{(i,j)}(t,\tau) = \sqrt{\mathcal{P}_p(t)} \times \sum_{q=0}^{Q_p(t)-1} \alpha_{p,q}^{(i,j)}(t) e^{j2\pi f_{\mathrm{D,p,q}}(t)t} \delta\big(\tau - \tau_{p,q}(t)\big)$$

$$\mathbf{h}_p^{(i,j)}(t,\tau) \approx \sqrt{\mathcal{P}_p} \sum_{q=0}^{Q_p-1} \alpha_{p,q}^{(i,j)} e^{j2\pi\epsilon_{\mathrm{D,p}}\Delta f t} \delta(\tau - \tau_{p,q}). \quad (1)$$

where $i \in \{0, 1, \cdots, N_{\mathrm{RX}} - 1\}, j \in \{0, 1, \cdots, N_{\mathrm{TX}} - 1\}$, $\mathcal{P}_p = 10^{-(\mathcal{P}_{\mathrm{d}} + \mathcal{P}_{\mathrm{S}})/10}$, $\mathcal{P}_{\mathrm{d}} = 20\log_{10}(4\pi d/\lambda)$ represents the large scale fading loss due to distance d between the satellite and p-th UE, $\mathcal{P}_{\mathrm{S}} \sim \mathcal{N}(0, \sigma_S^2)$ represents the shadowing with σ_S^2 variance. Whereas $q, Q_p, \alpha_{p,q}, \tau_{p,q}$ represents the index of the path, the total number of paths, small-scale path gain according to NTN-TDL-C and NTN-TDL-D [20], and

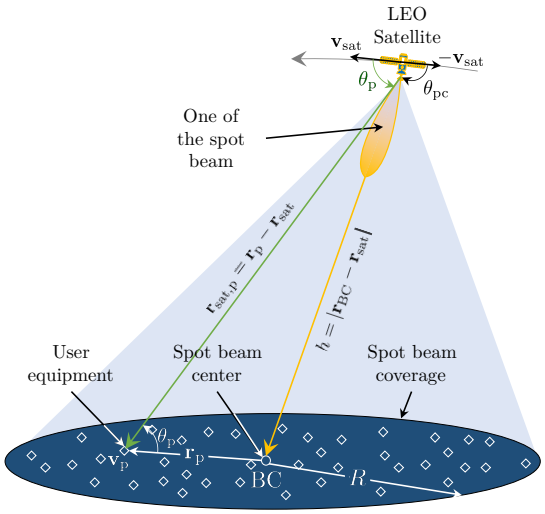

Fig. 1: Schematic of the system model, where $\mathbf{r}_{\mathrm{BC}}, \mathbf{r}_{\mathrm{p}}, \mathbf{r}_{\mathrm{sat}}$ are the relative position vector of the BC, UE, and satellite with respect to Earth. And $\mathbf{v}_{\mathrm{sat}}$ is relative velocity vector of the satellite with respect to Earth.

delay for the p-th UE and qth path respectively. Furthermore, $\epsilon_{\mathrm{D,p}} = f_{\mathrm{D,p}}/\Delta f$, is the normalized Doppler frequency with respect to OFDM Sub-Carrier-Spacing (SCS) denoted as Δf. $f_{\mathrm{D,p}}$ Doppler frequency resulting due to motion of satellite and UE. However, in (1), we have assumed a quasi-static channel that does not vary between the slots, which is justifiable due to the duration of the 5G NR slot [21]. Furthermore, the Doppler frequency at the p-th UE location can be expressed as $f_{\mathrm{D,p}} = (v_{\mathrm{p,sat}}/c) f_c \cos\theta_{\mathrm{p}}$, where $\mathbf{v}_{\mathrm{p,sat}} = \mathbf{v}_{\mathrm{sat}} - \mathbf{v}_{\mathrm{p}}$ is the relative velocity vector between the UE and satellite, $v_{\mathrm{p,sat}} = |\mathbf{v}_{\mathrm{p,sat}}|$ is the magnitude of relative velocity vector, $\mathbf{r}_{\mathrm{sat,p}} = \mathbf{r}_{\mathrm{p}} - \mathbf{r}_{\mathrm{sat}}$ is the relative position vector between the satellite and UE, and $|\mathbf{r}_{\mathrm{sat,p}}|$ is the magnitude of relative position vector. Whereas θ_{p} is angle between the direction of arrival of signal and the relative velocity vector, given as

$$\theta_{\mathrm{p}} = \cos^{-1} \frac{\mathbf{v}_{\mathrm{p,sat}} \cdot \mathbf{r}_{\mathrm{sat,p}}}{|\mathbf{v}_{\mathrm{p,sat}}||\mathbf{r}_{\mathrm{sat,p}}|}, \quad (2)$$

B. Satellite Transmitter Signal Model

We consider an OFDM signal supporting multiple SCS. The OFDM baseband equivalent model of the transmit signal can then be expressed as

$$\tilde{\mathbf{x}}[n] = \frac{1}{N} \sum_{k=0}^{N-1} \mathbf{X}[k] e^{j2\pi r n/N}. \quad (3)$$

For $n = -N_{\mathrm{CP}}, \cdots, N-1$. Where $N, N_{\mathrm{CP}}, \mathbf{X}[k]$ denotes FFT size, length of cyclic prefix, the rth sub-carrier symbol.

Doppler Pre-Compensated Signal: The satellite applies Doppler frequency pre-compensation to the OFDM signal before transmission, considering the BC location on Earth. The pre-compensated signal can be expressed mathematically

using (3) as

$$\begin{aligned}\mathbf{x}[n] &= \tilde{\mathbf{x}}[n]e^{\jmath 2\pi r\epsilon^{\text{pc}}_{\text{D,sat}}n/N} \\ &= \frac{1}{N}\sum_{k=0}^{N-1}\mathbf{X}[k]e^{\jmath 2\pi(r+\epsilon^{\text{pc}}_{\text{D,sat}})n/N},\end{aligned} \tag{4}$$

where $\epsilon^{\text{pc}}_{\text{D,sat}} = f^{\text{pc}}_{\text{D,sat}}/\Delta f$ is the pre-compensated normalized Doppler frequency, and $f^{\text{pc}}_{\text{D,sat}} = (v_{\text{sat}}/c)f_c\cos\theta_{\text{pc}}$, where θ_{pc} is the angle between the transmitted signal direction towards the BC and the negative of satellite velocity vector expressed as

$$\theta_{\text{pc}} = \cos^{-1}\frac{-\mathbf{v}_{\text{sat}}\cdot\mathbf{r}_{\text{sat,BC}}}{|\mathbf{v}_{\text{sat}}||\mathbf{r}_{\text{sat,BC}}|}, \tag{5}$$

where $v_{\text{sat}} = |\mathbf{v}_{\text{sat}}|, \mathbf{v}_{\text{sat}}, r_{\text{sat,BC}} = |\mathbf{r}_{\text{sat,BC}}|, \mathbf{r}_{\text{sat,BC}} = \mathbf{r}_{\text{BC}} - \mathbf{r}_{\text{sat}}$ is the magnitude of satellite velocity vector, satellite velocity vector and the relative position vector between the satellite and beam-center respectively. As shown in Fig. 2, the

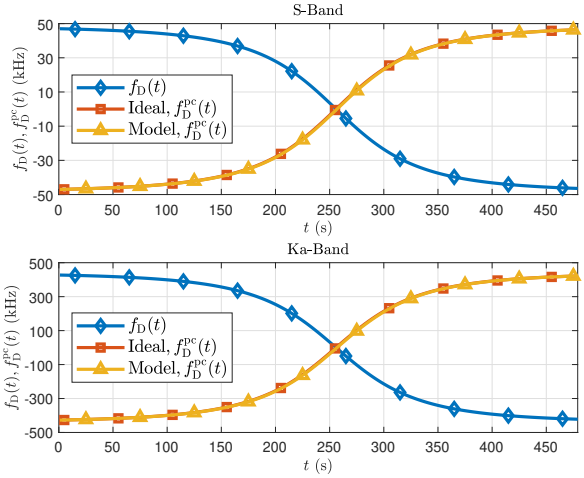

Fig. 2: Doppler frequency curve and satellite pre-compensated Doppler frequency

pre-compensated Doppler frequency complements the actual Doppler frequency. So the residual Doppler frequency at the BC will be zero in an ideal situation. But due to onboard attitude control and position determination errors, the satellite can introduce an error while pointing toward the BC, assuming an error to be within $U(-5, 5)$ km. Then the error introduced in the pre-compensated Doppler frequency can be seen.

C. User Terminal Received Signal Model

At the user terminal, we introduce the CFO denoted by f_{co}, impairment due to the mismatch between the transmitter and receiver local oscillators. Then the downlink received signal at the i-th receive antenna of the p-th UE at the n-th discrete time instant can be expressed as

$$\begin{aligned}\mathbf{y}^{(i)}_p[n] &= \sum_{j=0}^{N_T-1}\left(\mathbf{h}^{(i,j)}_p(n,m)\circledast\mathbf{x}^{(j)}[n]\right)\times e^{\jmath 2\pi\epsilon_{\text{co}}n/N} \\ &\quad + \mathbf{w}^{(i)}_p[n] \\ &= \sum_{j=0}^{N_T-1}\sqrt{\mathcal{P}_p}\sum_{q=0}^{Q_p-1}\alpha^{(i,j)}_{p,q}e^{\jmath 2\pi(\epsilon_{\text{D,p}}+\epsilon_{\text{co}})n/N} \\ &\quad \times\mathbf{x}^{(j)}[n-m_{p,q}] + \mathbf{w}^{(i)}_p[n],\end{aligned} \tag{6}$$

where $\mathbf{h}^{(i,j)}_p(n,m), \epsilon_{\text{co}} = f_{\text{co}}/\Delta f$ represents the discrete-time channel impulse response of (1), and the normalized CFO respectively, and $\mathbf{w}^{(i)}_p[n] \sim \mathcal{CN}(0,\sigma^2_w)$ is the complex white Gaussian noise modeled as complex Gaussian random variable with zero mean and variance σ^2_w. Whereas in the frequency domain, the received symbols can be expressed as

$$\begin{aligned}\mathbf{Y}^{(i)}_p[k] &= \sum_{n=0}^{N-1}\mathbf{y}^{(i)}_p[n]e^{-\jmath 2\pi kn/N} \\ &= \sum_{j=0}^{N_T-1}\frac{1}{N}\sum_{r=0}^{N-1}\mathbf{X}^{(j)}[r]e^{-\jmath 2\pi(r+\epsilon^{\text{pc}}_{\text{D,sat}})m_{p,q}/N} \\ &\quad\times\sqrt{\mathcal{P}_p}\sum_{q=0}^{Q_p-1}\alpha^{(i,j)}_{p,q}e^{\jmath\pi(r-k+\epsilon^{\text{res}})(1-1/N)} \\ &\quad\times\frac{\sin\{\pi(r-k+\epsilon^{\text{res}})\}}{\sin\{\pi(r-k+\epsilon^{\text{res}})/N\}} + \mathbf{W}^{(i)}_p[k],\end{aligned} \tag{7}$$

where in (7)

$$\epsilon^{\text{res}} = \epsilon^{\text{pc}}_{\text{D,sat}} + \epsilon_{\text{D,p}} + \epsilon_{\text{co}}, \tag{8}$$

is the normalized residual frequency. In case of flat fading with a single transmit and receive antenna (7) will be equivalent to [4].

III. Estimation, Post Compensation, and Detection

The UE will observe the residual frequency (7) at a distance d from the BC, which requires its estimation before post-compensation for proper synchronization. And since we want to assess the pre-compensation techniques, we assume that the UE is stationary and has a negligible CFO. Thus we rely on the estimation of residual frequency using CP, [22] from multiple symbols in a 5G slot i.e.

$$\hat{f}_0 = -\frac{\angle\{\mathbb{E}[\mathbf{y}_p[n]\mathbf{y}^*_p[n+N]]\}}{2\pi NT_s}, \tag{9}$$

where T_s is the sampling time and $\hat{f}_0$ is bounded within $\pm\Delta f/2$ [22]. However, correct estimation using (9) requires detecting the location of CP in an OFDM symbol for which we provide an Algorithm in 1. During the detection of CP location, there will be the possibility of false detection. This situation arises when $\mathbf{y}_p[n]$ and $\mathbf{y}_p[n+N]$ consists of noise. So we compute a threshold for the desired probability of false detection P_{FA}. Our simulation verified that the expression in

step 7 of Algorithm 1 follows the Rayleigh distribution. Thus for the desired P_{FA}, the threshold can be expressed as,

$$\beta_{\mathrm{CP}} = \sqrt{-2\eta \ln P_{\mathrm{FA}}}, \tag{10}$$

where η is the Rayleigh parameter, which can be evaluated using the Maximum Likelihood estimation as (11)

$$\eta = \frac{1}{2N} \sum_{l=0}^{N-1} \rho^2[l]. \tag{11}$$

After estimating the residual Doppler frequency, we can express the compensation of the received signal as (12).

$$\mathbf{y}_{c,p}^{(i)}[n] = \mathbf{y}_{p}^{(i)}[n] e^{-\jmath 2\pi \hat{f}_0 n}. \tag{12}$$

Algorithm 1 Residaul Doppler frequency estimation

Step 1: Set $\mathbf{y}_1^{(i)}[n] \leftarrow \mathbf{y}_p^{(i)}[n]$
Step 2: Get the portion of signal delayed by N, i.e. $\mathbf{y}_2^{(i)}[n] \leftarrow \mathbf{y}_p^{(i)}[n+N]$
Step 3: Compute the energy of each sample in both the signals, i.e., $E_{y1}^{(i)}[n] \leftarrow |\mathbf{y}_1^{(i)}[n]|^2$ and $E_{y2}^{(i)}[n] \leftarrow |\mathbf{y}_2^{(i)}[n]|^2$
Step 4: Compute correlation, i.e. $\mathbf{R}^{(i)}[n] \leftarrow \mathbf{y}_1^{(i)}[n]\mathbf{y}_2^{(i)*}[n]$
Step 5: Calculate the moving sum average for each N_{CP} samples across each receive antenna and discard samples from 1 to N_{CP}
$\mathbf{R}_{\mathrm{avg}}^{(i)}[n] \leftarrow \mathbf{R}^{(i)}[n] \circledast x_{\mathrm{CP}}[n]$
$E_{1,\mathrm{avg}}^{(i)}[n] \leftarrow E_{y1}^{(i)}[n] \circledast x_{\mathrm{CP}}[n]$
$E_{2,\mathrm{avg}}^{(i)}[n] \leftarrow E_{y2}^{(i)}[n] \circledast x_{\mathrm{CP}}[n]$,
where $x_{\mathrm{CP}}[n] = [1, \cdots, N_{\mathrm{CP}}]$
Step 6: Compute following
$\mathbf{R}_{\mathrm{avg}}[n] \leftarrow \sum_{i=0}^{N_{\mathrm{RX}}-1} \mathbf{R}_{\mathrm{avg}}^{(i)}[n]$,
$E_{1,\mathrm{avg}}[n] \leftarrow \sum_{i=0}^{N_{\mathrm{RX}}-1} E_{1,\mathrm{avg}}^{(i)}[n]$,
$E_{2,\mathrm{avg}}[n] \leftarrow \sum_{i=0}^{N_{\mathrm{RX}}-1} E_{2,\mathrm{avg}}^{(i)}[n]$
Step 7: Compute the normalized correlation as, $\rho[n] = |\mathbf{R}_{\mathrm{avg}}[n]| / \sqrt{E_{1,\mathrm{avg}}[n] E_{2,\mathrm{avg}}[n]}$
Step 8: Split $\rho[n]$ to N_s segment, where $N_s = \lceil N_{\mathrm{sample}}/N \rceil$
Step 9: Find the maximum for each segment, and select the peak location greater than the threshold using (10), and substitute those values to (9) for residual Doppler frequency estimation

A. Detection of Primary Synchronization Signal

After post-compensation of the received signal, the UE tries to detect the 5G NR primary synchronization signal (PSS). For which, UE performs the cross-correlation in the time domain with (12) and 5G NR PSS $\mathbf{x}_{\mathrm{PSS}}^{(\iota)}[n]$ for all possible values of physical layer cell ID [21], $\iota = N_{\mathrm{ID}}^{(2)} \in \{0, 1, 2\}$, and selecting the value which maximizes the peak of cross-correlation given then the threshold. i.e

$$\hat{\iota} = \max_{\iota} \left\{ \sum_{i=0}^{N_{\mathrm{RX}}-1} \left| \mathbf{\Lambda}_{\iota,i}[k] \right| \right\} > \beta_{\mathrm{PSS}}, \forall\ \iota, \tag{13}$$

where $\mathbf{\Lambda}_{\iota,i}[k], \beta_{\mathrm{PSS}}$ denotes the cross-correlation in (14) and threshold evaluated for the desired probability of false alarm (15) respectively.

$$\mathbf{\Lambda}_{\iota,i}[k] = \sum_{n=0}^{N-1} \mathbf{x}_{\mathrm{PSS}}^{(\iota)}[n] \mathbf{y}_{c,p}^{(i)*}[n-k]. \tag{14}$$

However, the detector can falsely detect the PSS when the corresponding OFDM symbol does not contain PSS. Hence in the absence of PSS, the received signal is Gaussian noise, i.e., $\mathbf{y}_{c,p}^{(i)}[n] = \mathbf{w}_p^{(i)}[n]$. So the probability of a false alarm can be evaluated as

$$\begin{aligned} P_{\mathrm{FA}} &= \Pr\left\{ \sum_{i=0}^{N_{\mathrm{RX}}-1} \left| \mathbf{\Lambda}_{\iota,i}[k] \right| > \beta_{\mathrm{PSS}} \right\} \\ &= \Pr\left\{ Y > \beta_{\mathrm{PSS}} \right\} \\ &= 1 - F_Y(\beta_{\mathrm{PSS}}) \\ \beta_{\mathrm{PSS}} &= F_Y^{-1}(1 - P_{\mathrm{FA}}). \end{aligned} \tag{15}$$

where $Y = \sum_{i=0}^{N_{\mathrm{RX}}-1} \left| \mathbf{\Lambda}_{\iota,i}[k] \right|$. Fig. 3 shows our simulation; it has been verified that the random variable Y follows the Nakagami distribution, i.e., $Y \sim \mathrm{Nakagami}(m, \Omega)$, where m, Ω can be computed directly from the Y as, $m = (\mathbb{E}[Y^2])^2 / \mathbb{V}ar[Y^2]$ and $\Omega = \mathbb{E}[Y^2]$

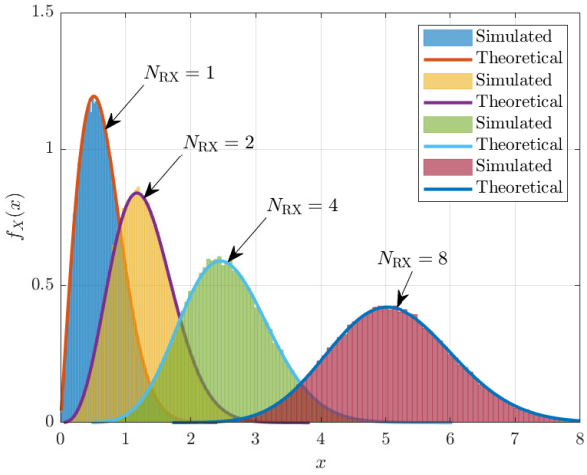

Fig. 3: Accuracy of distribution function

IV. Results and Discussions

In this section, we discuss the outcomes derived from the Monte Carlo simulations of our proposed method. Table I presents the simulation parameters.

A. Maximum residual Doppler frequency and maximum range

We evaluate the expression to ascertain the maximum range needed to accurately estimate the maximum residual Doppler frequency within a desired maximum CFO receiver can estimate efficiently. Furthermore, we assume that the UE is stationary and has negligible CFO. Thus, the maximum residual Doppler shift is observed when the pre-compensated Doppler frequency approaches zero. This situation arises when the angle between the direction of arrival of the signal at the

BC and the satellite's velocity vector reaches 90°. Therefore from (8), let $f_{\mathrm{D,max}}^{\mathrm{res}}$ represents the maximum residual Doppler frequency, then

$$f_{\mathrm{D,max}}^{\mathrm{res}} = f_{\mathrm{D}}^{\mathrm{p}} = \frac{v_{\mathrm{p,sat}}}{c} f_c \cos\theta_{\mathrm{p}} = \frac{v_{\mathrm{sat}}}{c} f_c \cos\theta_{\mathrm{p}}. \tag{16}$$

From Fig. 1, we can use the definition of $\cos\theta_{\mathrm{p}}$ in (16), on solving for R and set the maximum residual Doppler frequency to be half of the SCS as $\hat{f}_0$ of (9) in bounded within half of the SCS leads to

TABLE I: Simulation Parameters

Satellite Orbital Elements	Semimajor Axis, $\alpha = 6970000$ Eccentricity, $e = 0$ Inclination, $i = 0°$ RAAN, $\Omega = 0°$ Argument of periapsis, $\omega = 0°$ True Anomaly, $v = 0°$
Minimum elevation angle	10°
Beam center location	Latitude: -0.0010703823211031874 Longitude: 34.59977641558434
Error in pointing	$\mathrm{U}(-5, 5)$ (km)
Frequency band	S-Band, Ka-band
Carrier Frequency	$f_c = 2.2, 20$ (GHz)
Minimum Bandwidth	7.2, 28.8 (MHz)
Sub-carrier spacing	30, 120 (kHz)
5G NR Downlink Signal	Synchronization Signal Block (SSB)
Tapped Delay Line	NTN TDL-D
Shadowing Standard Deviation	5 (dB)
Probability of false alarm, P_{FA}	1/100

$$R \leq \sqrt{\frac{h^2}{\left(\frac{2v_{\mathrm{sat}} f_c}{c\Delta f}\right)^2 - 1}}, \tag{17}$$

where R is the maximum range of the beam coverage, and h

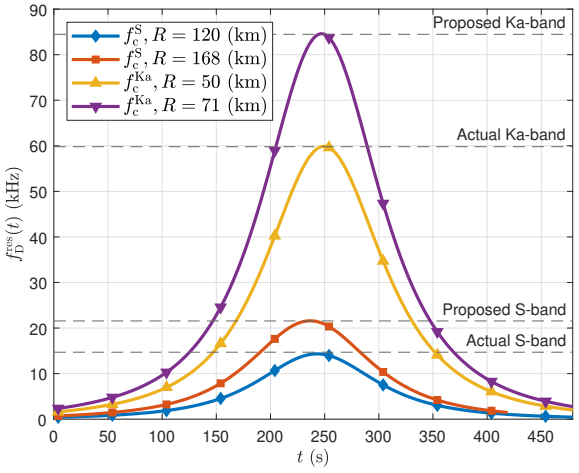

Fig. 4: Maximum residual Doppler frequency, where $f_{\mathrm{c}}^{\mathrm{S}} = 2.2$ (GHz) and $f_{\mathrm{c}}^{\mathrm{Ka}} = 20$ (GHz)

is the satellite's altitude. The expression in (17) is calculated assuming the Earth and the satellite's orbit is in two parallel planes. Nevertheless, it is essential to acknowledge that the proposed maximum range differs from the actual because it does not account for the curvature of the Earth. As shown in Fig. 4 for a satellite positioned at 558 km, moving at a velocity of 7.08 km/s, according to (17), the proposed maximum range satisfying (9) can be achieved in the S and Ka-band, with an SCS of 30 and 120 kHz, would be 168 and 71 km, respectively. However, in actual scenarios reduce these values to approximately 120 and 50 km. Furthermore, if we relax the assumption of negligible CFO and UE mobility, then (17) will be

$$R \leq \sqrt{\frac{h^2}{\left(\frac{v_{\mathrm{sat}} f_c}{c f_{\mathrm{max}}^{\mathrm{res}}}\right)^2 - 1}}, \tag{18}$$

where $f_{\mathrm{max}}^{\mathrm{res}} = f_{\mathrm{D,p}} + f_{\mathrm{co}}$. But, it will require coarse CFO estimation at the UE.

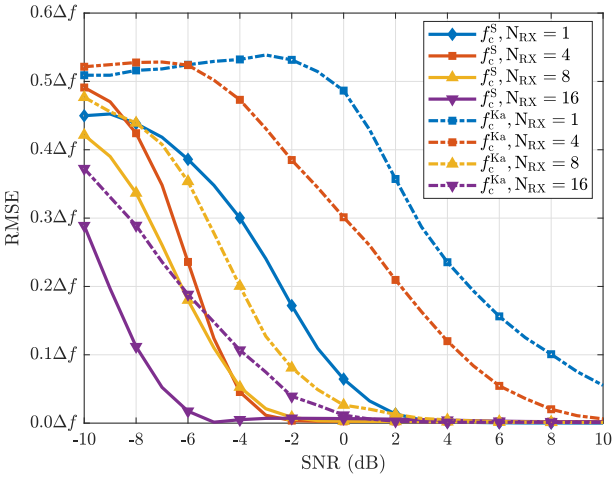

Fig. 5: Estimation of residual Doppler frequency, where $f_{\mathrm{c}}^{\mathrm{S}} = 2.2$ (GHz) and $f_{\mathrm{c}}^{\mathrm{Ka}} = 20$ (GHz)

B. Root Mean Square Error (RMSE) of maximum residual Doppler frequency estimation

Here we discuss the RMSE of normalized maximum residual Doppler frequency estimation versus SNR for the UE equipped with different numbers of receive antennas. To examine the performance of our Algorithm 1, we use the maximum residual Doppler frequency for S- and Ka-band, i.e., $f_{\mathrm{D,max}}^{\mathrm{res}} = [14.32\ (\mathrm{kHz}), 59.34\ (\mathrm{kHz})]$ respectively as seen from Fig. 4. As shown in Fig. 5, the RMSE of the frequency estimation starts decreasing for the higher SNR level. However, we observe a little deviation for low SNR and spatial diversity. As the number of receiving antennas increases, the performance also improves. However, a UE operating in S-band attains negligible RMSE as the SNR increases, but the UE in Ka-band still requires a gain of 7 dB SNR for a single receive antenna. Moreover, as the receive antenna increases, the gain in SNR also reduces. It is because, as the SCS increases, the slot duration decreases; consequently, the duration of the cyclic prefix also decreases, which should have provided a better estimation, but the effect of Doppler tends to be higher in Ka-band. Nevertheless, it can be improved by considering multiple slots for higher SCS with the same duration as lower SCS. Also, as discussed in the next section, this does not prevent the UE from detecting the PSS.

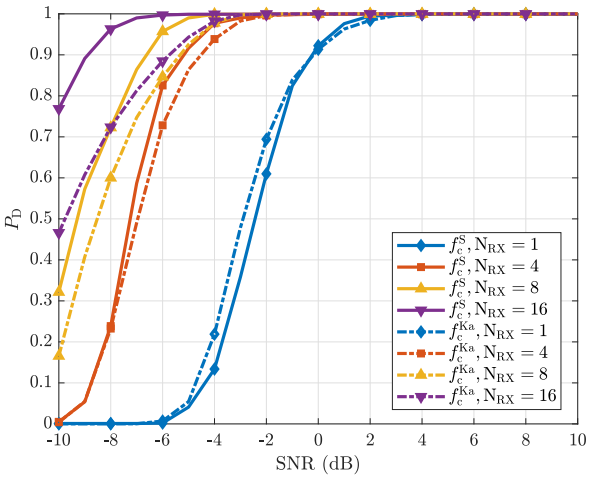

Fig. 6: Probability of detection of PSS, where $f_c^S = 2.2$ (GHz) and $f_c^{Ka} = 20$ (GHz)

C. Probability of detection of PSS

This study investigated the 5G NR PSS detection probability concerning the maximum residual Doppler frequency and SNR in both S- and Ka-bands. The results, depicted in Fig. 6, reveal that even though estimating the residual Doppler frequency for the Ka-band required a higher SNR, the probability of detecting PSS showed minimal difference compared to the S-band. This similarity is because the maximum residual Doppler frequency remained well within the bounds of estimation capabilities. Moreover, the 5G NR PSS exhibits favorable auto-correlation properties, enabling accurate detection and synchronization even with small frequency offsets. However, there is a trade-off: the Ka-band exhibited a smaller beam coverage range than the S-band. Despite this, the study demonstrates that UE equipped with at least four receive antennas can satisfactorily detect PSS and achieve initial synchronization with LEO-based NTN gNB.

V. Conclusion and Future Work

This paper presents an efficient method to mitigate the Doppler effect in an LEO-based 5G NTN. The approach involves Doppler pre-compensation, eliminating the need for UE to possess satellite ephemeris during initial synchronization. As a result, the technique significantly improves the detection probability of PSS even in low SNR conditions. However, it was observed that estimating the residual Doppler frequency for the Ka-band requires a higher SNR level. The study proposes integer frequency offset estimation to address this limitation and further enhance the estimation range. Future work will explore scenarios with multiple spot beams serving UEs within different BC. However, this setup introduces a challenge at the edge, where interference from adjacent spot beam coverage may occur. Joint Doppler and interference mitigation techniques will be necessary to handle this situation effectively.

References

[1] X. Lin, S. Rommer, S. Euler, E. A. Yavuz, and R. S. Karlsson, "5G from space: An overview of 3GPP Non-Terrestrial Networks," *IEEE Communications Standards Magazine*, vol. 5, no. 4, pp. 147–153, 2021.

[2] M. M. Azari, S. Solanki, S. Chatzinotas, O. Kodheli, H. Sallouha, A. Colpaert, J. F. Mendoza Montoya, S. Pollin, A. Haqiqatnejad, A. Mostaani, E. Lagunas, and B. Ottersten, "Evolution of non-terrestrial networks from 5G to 6G: A survey," *IEEE Communications Surveys Tutorials*, vol. 24, no. 4, pp. 2633–2672, 2022.

[3] F. Rinaldi, H.-L. Maattanen, J. Torsner, S. Pizzi, S. Andreev, A. Iera, Y. Koucheryavy, and G. Araniti, "Non-terrestrial networks in 5G & beyond: A survey," *IEEE access*, vol. 8, pp. 165 178–165 200, 2020.

[4] P. Moose, "A technique for orthogonal frequency division multiplexing frequency offset correction," *IEEE Transactions on Communications*, vol. 42, no. 10, pp. 2908–2914, 1994.

[5] "3GPP TR 38.821, "3rd generation partnership project; technical specification group radio access network; solutions for NR to support non-terrestrial networks (NTN) (release 16)," 2021.

[6] I. Ali, N. Al-Dhahir, and J. Hershey, "Doppler characterization for LEO satellites," *IEEE Transactions on Communications*, vol. 46, no. 3, pp. 309–313, 1998.

[7] J. Lin, Z. Hou, Y. Zhou, L. Tian, and J. Shi, "MAP estimation based on doppler characterization in broadband and mobile LEO satellite communications," in *2016 IEEE 83rd Vehicular Technology Conference (VTC Spring)*, 2016, pp. 1–5.

[8] A. Guidotti, A. Vanelli-Coralli, M. Caus, J. Bas, G. Colavolpe, T. Foggi, S. Cioni, A. Modenini, and D. Tarchi, "Satellite-enabled LTE systems in LEO constellations," in *2017 IEEE International Conference on Communications Workshops (ICC Workshops)*, 2017, pp. 876–881.

[9] W. Wang, Y. Tong, L. Li, A.-A. Lu, L. You, and X. Gao, "Near optimal timing and frequency offset estimation for 5G integrated LEO satellite communication system," *IEEE Access*, vol. 7, pp. 113 298–113 310, 2019.

[10] M. Conti, S. Andrenacci, N. Maturo, S. Chatzinotas, and A. Vanelli-Coralli, "Doppler impact analysis for NB-IoT and satellite systems integration," in *ICC 2020 - 2020 IEEE International Conference on Communications (ICC)*, 2020, pp. 1–7.

[11] M. Huang, J. Chen, and S. Feng, "Synchronization for OFDM-based satellite communication system," *IEEE Transactions on Vehicular Technology*, vol. 70, no. 6, pp. 5693–5702, 2021.

[12] D. Nieto Yll, "Doppler shift compensation strategies for LEO satellite communication systems," Ph.D. dissertation, UPC, Escola Tècnica Superior d'Enginyeria de Telecomunicació de Barcelona, Departament de Teoria del Senyal i Comunicacions, Jun 2018. [Online]. Available: http://hdl.handle.net/2117/123510

[13] D. Tian, Y. Zhao, J. Tong, G. Cui, and W. Wang, "Frequency offset estimation for 5G based LEO satellite communication systems," in *2019 IEEE/CIC International Conference on Communications in China (ICCC)*, 2019, pp. 647–652.

[14] M. Pan, J. Hu, J. Yuan, J. Liu, and Y. Su, "An efficient blind doppler shift estimation and compensation method for LEO satellite communications," in *2020 IEEE 20th International Conference on Communication Technology (ICCT)*, 2020, pp. 643–648.

[15] J. Wang, C. Jiang, L. Kuang, and B. Yang, "Iterative doppler frequency offset estimation in satellite high-mobility communications," *IEEE Journal on Selected Areas in Communications*, vol. 38, no. 12, pp. 2875–2888, 2020.

[16] X. Lin, Z. Lin, S. E. Löwenmark, J. Rune, R. Karlsson, and Ericsson, "Doppler shift estimation in 5G new radio non-terrestrial networks," in *2021 IEEE Global Communications Conference (GLOBECOM)*, 2021, pp. 1–6.

[17] S. Kumar, A. Astro, O. Kodheli, J. Querol, S. Chatzinotas, T. Schlichter, G. Casati, T. Heyn, F. Völk, S. Kaya *et al.*, "5G-NTN GEO-based in-lab demonstrator using openairinterface5G," in *11th Advanced Satellite Multimedia Conference*, 2022.

[18] S. Kumar, A. K. Meshram, A. Astro, J. Querol, T. Schlichter, G. Casati, T. Heyn, F. Völk, R. T. Schwarz, A. Knopp *et al.*, "Openairinterface as a platform for 5G-NTN research and experimentation," in *2022 IEEE Future Networks World Forum (FNWF)*. IEEE, 2022, pp. 500–506.

[19] Z. M. Cross, Paul, "LEO GPS Attitude Determination Algorithm Designed for Real-time On-board Execution — ion.org," https://www.ion.org/publications/abstract.cfm?articleID=2111, [Accessed 28-07-2023].

[20] "3GPP TR 38.811, "3rd generation partnership project; technical specification group radio access network; study on new radio (NR) to support non-terrestrial networks (release 15)," 2020-09.

[21] "3GPP TS 38.211, "NR; Physical channels and modulation." 3rd Generation Partnership Project; Technical Specification Group Radio Access Network. (release 17.4.0)," 2023-01.

[22] J. van de Beek, M. Sandell, and P. Borjesson, "Ml estimation of time and frequency offset in OFDM systems," *IEEE Transactions on Signal Processing*, vol. 45, no. 7, pp. 1800–1805, 1997.